Journal of Power Sources 597 (2024) 234106

Contents lists available at ScienceDirect

Journal of Power Sources

journal homepage: www.elsevier.com/locate/jpowsour

The battery failure databank: Insights from an open-access database of thermal runaway behaviors of Li-ion cells and a resource for benchmarking risks

Donal P. Finegan [a,*], Julia Billman [a], Jacob Darst [b], Peter Hughes [b], Jesus Trillo [b], Matt Sharp [a], Alex Benson [a], Martin Pham [c], Inez Kesuma [c,f], Mark Buckwell [c,f], Hamish T. Reid [c], Charlie Kirchner-Burles [c,f], Matilda Fransson [c], David Petrushenko [b], Thomas M.M. Heenan [c,f], Rhodri Jervis [c,f], Rhodri Owen [c,f], Drasti Patel [c], Ludovic Broche [d], Alexander Rack [d], Oxana Magdysyuk [e], Matt Keyser [a], William Walker [b], Paul Shearing [c,f,g], Eric Darcy [b]

[a] National Renewable Energy Laboratory, 15013 Denver W. Parkway, Golden, CO, 80401, USA
[b] National Aeronautics and Space Administration, Johnson Space Center, 2101 E NASA Pkwy, Houston, TX, 77058, USA
[c] Electrochemical Innovation Laboratory, University College London, Torrington Place, London, WC1E7JE, UK
[d] ESRF – The European Synchrotron, 71 Avenue des Martyrs, 38000, Grenoble, France
[e] Diamond Light Source, Harwell Science and Innovation Campus, Fermi Ave, Didcot OX11 0DE, UK
[f] The Faraday Institution, Harwell Campus, Didcot, OX11 0RA, UK
[g] The ZERO Institute, University of Oxford, Holywell House, Osney Mead, Oxford, OX2 0ES, UK

A B S T R A C T

The thermal response of Li-ion cells can greatly vary for identical cell designs tested under identical conditions, the distribution of which is costly to fully characterize experimentally. The open-source Battery Failure Databank presented here contains robust, high-quality data from hundreds of abuse tests spanning numerous commercial cell designs and testing conditions. Data was gathered using a fractional thermal runaway calorimeter and contains the fractional breakdown of heat and mass that was ejected, as well as high-speed synchrotron radiography of the internal dynamic response of cells during thermal runaway. The distribution of thermal output, mass ejection, and internal response of commercial cells are compared for different abuse-test conditions, which when normalized on a per amp-hour basis show a strong positive correlation between heat output from cells, the fraction of mass ejected from the cells, their energy- and power-density. Ejected mass was shown to contain 10 × more heat per gram than non-ejected mass. The causes of 'outlier' thermal and ejection responses i.e., extreme cases, are elucidated by high-speed radiography which showed how occurrences such as vent clogging can create more hazardous conditions. High-speed radiography also demonstrated how the time-resolved interplay of thermal runaway propagation and mass ejection influences the total heat generated.

1. Introduction

Lithium (Li)-ion batteries are an energy-storage solution for a wide range of applications including electric vehicles, grid-scale energy storage, and portable electronics. This is largely due to performance improvements and cost reductions over the past decade and this trend is expected to continue [1]. With increasing reliance on Li-ion batteries, the fallout of catastrophic failure of batteries can be severe, as demonstrated by grounding of an entire fleet of aircraft [2], and the recall of an entire product line of smart-phones [3]. When a battery reaches certain temperature thresholds, exothermic reactions occur with increasing rates of heat generation at elevated temperatures. When heat generation exceeds heat dissipation from the cell, thermal runaway can ensue causing hazardous conditions that can propagate throughout modules [4]. Electric vehicle researchers from Volkswagen and Ford emphasized the importance of more detailed and cost-effective testing and modelling methods for understanding the risks posed by thermal runaway to design safer battery systems [5,6]. To achieve this, there is a clear need for broad access to robust, high-quality, and relevant experimental data on battery failure to support interdisciplinary efforts to improve battery safety.

When a cell undergoes thermal runaway, a series of exothermic reactions propagate throughout the cell within fractions of a second [7,8], which is observed externally as hot flares and violent ejection. This is

* Corresponding author.
E-mail address: donal.finegan@nrel.gov (D.P. Finegan).

https://doi.org/10.1016/j.jpowsour.2024.234106
Received 25 October 2023; Accepted 17 January 2024
Available online 1 February 2024

particularly hazardous for cylindrical cells that risk pressure-induced ruptures due to the design facilitating a build-up of pressure [9]. Different types (manufacturer and model) of Li-ion cells behave differently during thermal runaway [10] and recent work has shown that identical cells repeatedly tested under identical abuse conditions, can display a distribution of heat output and temperatures [11,12], demonstrating the need for conducting several repeat tests and statistical analyses of the variable battery failure data. This variable behavior challenges the ability of deterministic modelling methods to predict the risks associated with battery failure. Despite deterministic models being guided by experimental data [13–16], there remains some uncertainty on the statistical behavior of the specific cell and how it will behave under slightly different abuse conditions. Furthermore, experimental methods used to validate models do not represent the complex behavior of cells undergoing failure. For example, calorimetry methods measure the total heat output from a cell, but do not capture the fraction of heat ejected from the cell, which is an important detail for engineers to consider when designing a battery system.

The Fractional Thermal Runaway Calorimeter (FTRC) developed by the authors [11] is capable of distinctly measuring ejected and non-ejected heat and mass. The FTRC also facilitates simultaneous radiography, giving insight into the link between rapid dynamic phenomena that occur within the cell during thermal runaway and the risks posed externally, thus helping identify the causes of catastrophic failure mechanisms. However, even with appropriate experimental techniques, understanding the variable behavior requires exhaustive testing, which is time consuming and costly. Computational methods are much less time consuming, but 3D multiphysics models can be very computationally intensive and require experimental validation. Recently, some research groups have explored the combination of machine-learning with different degrees of model complexities to rapidly explore large parameter spaces of abuse testing. For example, Kriston et al. [17] applied principle component analysis to data from 780 simulations to identify the most influential factors for creating a high likelihood of thermal runaway, and Li et al. [18] conducted 2500 simulations and used machine learning to identify a safety envelope for specific mechanical indentation conditions. However, while large parameter spaces are relatively cost-effective to explore in virtual space, they are costly to validate and explore in experimental space, thus making validation extremely challenging. This creates a clear need for large, high-quality, and relevant open-source databases on battery failure [19,20].

The application of machine learning methods applied to electrochemical data has recently demonstrated success for life-time predictions of cycling cells [21,22] and has helped quickly identify optimal charging protocols [23]. Efforts for predictive analyses of cycle life are also aided by open-source electrochemical data [21,24]. Another useful aspect of open-source datasets is the ability to benchmark new technologies against previous technologies [25]. The National Renewable Energy Laboratory (NREL) and National Aeronautics and Space Administration (NASA) have made data from hundreds of FTRC tests open access [26]. While large datasets of the thermal behavior of cells during thermal runaway have been published before, for example by groups at NREL [12], NASA [11], and Tsinghua University [27], none have provided the detail of the FTRC, high number of tests, simultaneous high-speed radiography, broad overview of various commercial cell models and abuse types, that the Battery Failure Databank (BFD) presented in this work does [26]. Here, data from hundreds of FTRC tests is drawn from the BFD to quantitatively show the distribution of failure scenarios that can occur for different commercial cell types under different abuse conditions. Correlations were found between the fraction of mass ejected and the total heat output from the cell, as well as correlations between the energy density (Wh/kg) and power density (W/kg) of cells and their normalized thermal response during thermal runaway. Furthermore, the causes of 'outlier' cells, the thermal response of which significantly deviates from the mean, are elucidated by exploring the high-speed radiography data that was simultaneously recorded during the FTRC tests. The statistical measurements in this work are expected to clarify the deficiencies in current experimental and modeling methods to capture the intricate detail of thermal runaway, as well as provide researchers and engineers with a valuable resource for future model validation and benchmarking of the relative thermal responses of current and future cell designs.

2. Methods

2.1. Fractional thermal runaway calorimetry

The FTRC, described in detail in previous work [11] and shown in Fig. 1a, was designed to measure the thermal runaway (TR) response of multiple cylindrical cell designs, including 18650, 21700, and D-cell formats. The FTRC can determine both the total heat released during thermal runaway, and the fractions of heat released through the cell casing and through the ejected material from the positive and negative ends of cylindrical cells. The FTRC uses a series of aluminum baffles, copper mesh, and exhaust end caps to capture ejected particles and arrest flames. This allows the total heat output to be determined from the total energy yield consisting of distinct measurements for heat from material ejected via the positive end of the cell, heat from the cell body, and heat from material ejected from the negative end of the cell.

Thermal runaway was induced for each cell using 3 different methods: (1) thermal abuse, where the cell was heated until thermal runaway occurred, (2) thermal abuse where the cell contained an internal short circuiting (ISC) device [7,28] and thus thermal runaway occurred at a considerably lower temperature than otherwise, and (3) nail penetration abuse. The ISC device consists of a copper and aluminum pad separated by a wax layer that is built into the electrodes of the cells [7]. It mimics short circuits induced by latent defects and can initiate thermal runaway in desired locations inside the cell, both radially and longitudinally, when the cell reaches about 57 °C [12]. Method (1) is referred to throughout the text as "thermal non-ISC" and method (2) is referred to as "thermal ISC" to distinguish when cells contained an ISC device. Nail penetration was facilitated using an adaptor on the FTRC that employed a pneumatically activated nail that travelled 9 mm into the cell body.

After each test, the FTRC was disassembled and the remaining mass from each section of the FTRC (positive ejected, cell body, and negative ejected) was recorded and tabulated in the Battery Failure Databank (BFD). The difference in mass collected post-thermal runaway and the original mass of the cell pre-thermal runaway was recorded as "unrecovered mass" and is thought to be mostly gas and smoke.

2.2. High-speed synchrotron X-ray imaging

Being made from aluminum, a material with low X-ray attenuation, the FTRC also facilitated simultaneous X-ray imaging leading up to and during thermal runaway. High-speed X-ray imaging provided insight into the internal dynamics of the cells during thermal runaway and was captured at The European Synchrotron (ESRF) beamline ID19 and the Diamond Light Source (DLS) synchrotron beamline I12 over several beamtimes spaced out over many years. In general, X-ray images were captured at 2000 or 3000 frames per second (fps) using a polychromatic beam. Radiography videos are provided as YouTube hyperlinks in the BFD and the imaging conditions for each specific test can be found at those hyperlinks. The radiography videos were processed using MATLAB's 'adapthisteq' function to enhance image contrast, and flat field corrections to remove artifacts. Radiographs were timestamped according to their frame rates.

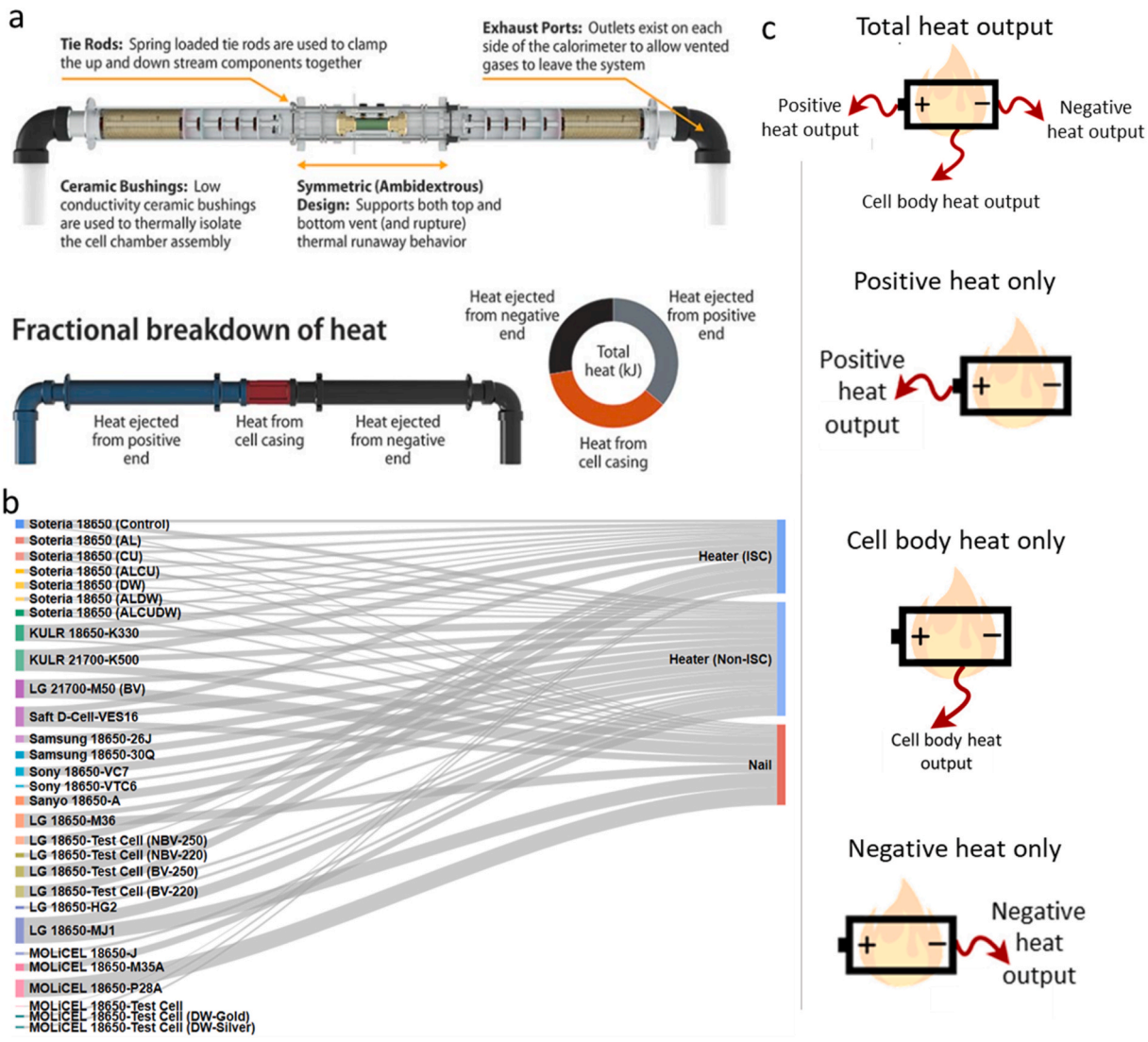

Fig. 1. (a) Illustration showing the design and function of the fractional thermal runaway calorimeter (FTRC) used for all experiments. (b) Sankey diagram showing the contents of the Battery Failure Databank (BFD) and breakdown of cell types and abuse methods. (c) Illustrations that will be used throughout the manuscript to help identify when heat measurements consist of total heat (positive ejected + cell body + negative ejected) or distinct heat measurements for positive ejected, cell body, or negative ejected.

3. Results and discussion

3.1. Contents of the battery failure databank (BFD)

Thermal and mass ejection data from 364 FTRC tests on cylindrical batteries are contained in this databank. Some of the tests were conducted at synchrotron facilities and are accompanied by in-situ high-speed radiography movies that are hyperlinked to YouTube. The cell types (models and manufacturers) and distribution of abuse types are shown in Fig. 1b. Most cells in the BFD are off-the-shelf commercial cells, but some of the cells are non-commercial "test-cells" that contain exploratory materials, such as the Soteria cells that contain combinations (i.e. on either one electrode or both electrodes) of current collectors with metallized polymer substrates and thermally stable cellulose separators. There are also some cells at varying state-of-charge (SOC) in the BFD, which will not be included in the scope of this manuscript. This rich assortment of cell types across different abuse methods and cell manufactures provides a valuable benchmark for comparisons.

Since the FTRC thermal and mass measurements consist of 3 distinct groupings (i.e., heat and mass from (1) positive ejected material, (2) the cell body, and (3) negative ejected material), illustrations are used to clarify what the data in each plot represents, as shown in Fig. 1c. The illustrations show when the total heat/mass (i.e., positive + cell body + negative) is being conveyed, or when any of the distinct measurements are being conveyed (i.e., positive or cell body or negative). These illustrations will be included on all plots throughout the manuscript.

For this manuscript, we focus on commercial or near-commercial cells at 100 % SOC. Therefore, custom-made cells with Soteria materials and cells at a SOC of less than 100 % will not be included in this work. This helps reduce variables and maintain focus on the high-risk scenarios posed by commercial cells at 100 % SOC that are most important to understand for battery pack designers to ensure their systems are safe. The cells that are included in this manuscript and their properties are shown in Table 1.

3.2. Trends in heat output from cells for different abuse types

The total energy output (kJ) of the cells during thermal runaway varied significantly for the different cell types and appears to have increased somewhat linearly with capacity, as shown in Fig. 2a. However, the linear trend is likely due to most cells having similar active material chemistries of graphite vs. $LiNiMnCoO_2$ (NMC) or $LiNiCoAlO_2$

Table 1
Properties of analyzed cells.

Cell Model	State of charge (%)	Voltage (V)	Capacity (Ah)	Casing thickness (μm)	Bottom vent (Y/N)	Max discharge rate (C)
KULR 18650-K330	100	4.1	3.3	220	Yes	2.0
KULR 21700-K500	100	4.1	5.0	220	Yes	2.0
LG 18650-HG2	100	4.1	3.0	150	No	6.7
LG 18650-M36	100	4.1	3.4	220	No	2.9
LG 18650-MJ1	100	4.1	3.5	165	No	2.9
LG 18650-Test Cell (BV-220)	100	4.1	3.4	220	Yes	2.9
LG 18650-Test Cell (BV-250)	100	4.1	3.4	250	Yes	2.9
LG 18650-Test Cell (NBV-220)	100	4.1	3.4	220	No	2.9
LG 18650-Test Cell (NBV-250)	100	4.1	3.4	250	No	2.9
LG 21700-M50 (BV)	100	4.1	5.0	250	Yes	1.5
MOLiCEL 18650-J	100	4.1	2.4	165	No	2.1
MOLiCEL 18650-M35A	100	4.1	3.4	Unknown	No	4.0
MOLiCEL 18650-P28A	100	4.1	2.6	Unknown	No	13.5
MOLiCEL 18650-Test Cell	100	4.1	2.4	Unknown	No	2.1
MOLiCEL 18650-Test Cell (DW-Gold)	100	4.1	2.4	Unknown	No	2.1
MOLiCEL 18650-Test Cell (DW-Silver)	100	4.1	2.4	Unknown	No	2.1
Panasonic 18650-BE	100	4.1	3.2	Unknown	No	2.0
Saft D-Cell-VES16	100	4.1	4.5	380	No	4.4
Samsung 18650-26J	100	4.1	2.6	Unknown	No	2.0
Samsung 18650-30Q	100	4.1	3.0	250	No	5.0
Sanyo 18650-A	100	4.1	2.1	Unknown	No	2.0
Sony 18650-VC7	100	4.1	3.5	Unknown	Yes	2.3
Sony 18650-VTC6	100	4.1	3.1	Unknown	No	4.8

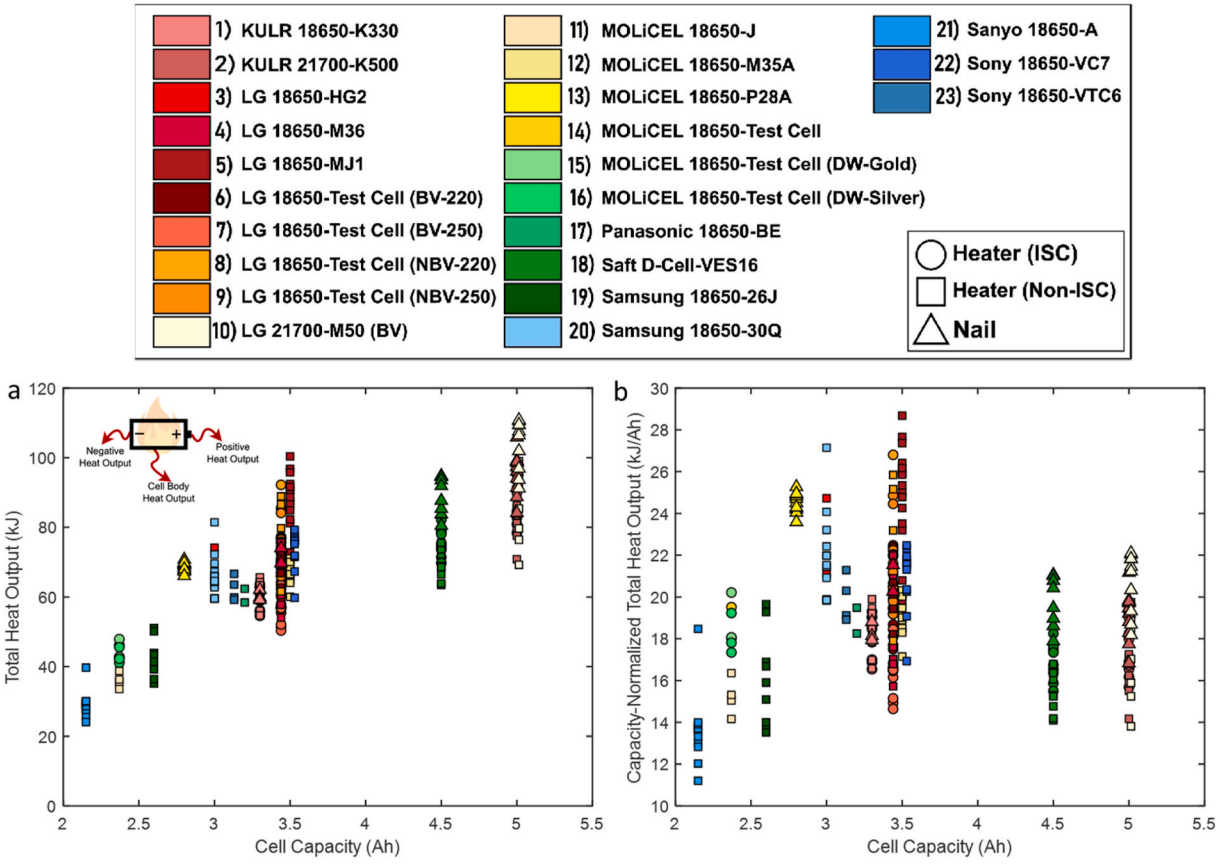

Fig. 2. (a) Total heat output as a function of cell capacity (100 % SOC at 4.1 V). (b) Total heat output normalized to cell capacity as a function of cell capacity.

(NCA). When normalized based on capacity to kJ/Ah in Fig. 2b, one would expect a convergence around a single value, but there is not only considerable variability for each cell type, but also between cell types, covering a large range from 12 kJ/Ah to 28 kJ/Ah. The differences between the variation of kJ/Ah from the different cells highlights the importance of evaluating the thermal runaway behavior of a sufficiently high number cells to fully characterize their thermal behavior. For example, the LG MJ1 cell displayed a minimum heat output of ~20 kJ/Ah and a maximum of ~29 kJ/Ah i.e., a 45 % increase from the minimum value. The plot in Fig. 2b also demonstrates the risk per Ah gained from each cell with some cells such as the Sanyo 18650-A showing an average of ~13 kJ/Ah and the LG MJ1 and MOLICEL P28A showing an average of ~25 kJ/Ah, almost twice as much heat to manage during thermal runaway per useable Ah of capacity. Most other cells displayed

an average of ~18 kJ/Ah.

In Table 1, the power capability of each cell is conveyed via the manufacturer's maximum continuous discharge rate, which varies between cells from 1.5 C (full discharge in 40 min) to 13 C (full discharge in just under 5 min). Typically, cells with higher discharge rates have thinner electrode coatings and consequently a higher ratio of inactive materials to active materials inside the cell i.e., more current collector mass per unit mass of active electrode material. We explored whether this difference in inactive/active ratio leads to any significant difference in heat or mass output. The ability to discharge quickly means that the battery can sustain higher currents and produce harder shorts during failure. Additionally, there may also be more surface area per unit capacity due to electrode particles being smaller and having higher specific areas to accommodate higher lithium fluxes, as well as other engineering changes.

Cells that are considered high-power cells in this matrix are the Samsung 30Q, Sony VTC6, MOLICEL P28A, and the LG HG2. The average energy released by the Samsung-30Q, MOLICEL P28A, and LG HG2 cells was around 23–25 kJ/Ah, which is around 33 % higher than the overall cell average of ~18 kJ/Ah. However, the Sony VTC6 cells produced around 20 kJ/Ah which is still greater than but considerably closer to the overall average. Therefore, on average, the cells with greater maximum discharge rates released greater amounts of heat per Ah.

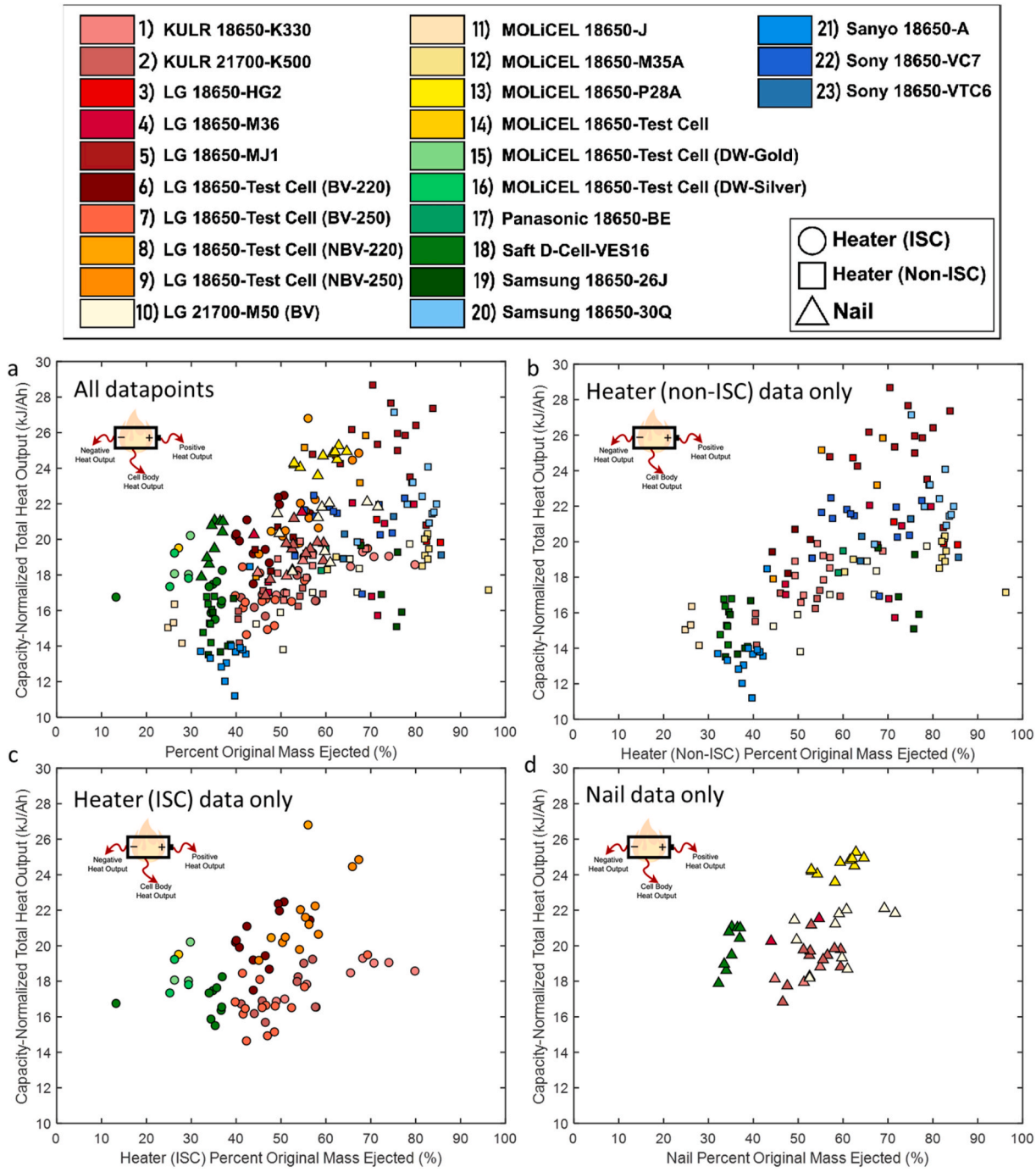

Fig. 3. Capacity-normalized heat output as a function of percent mass ejected from the cell for (a) all test data, (b) only heater (non-ISC) abuse tests, (c) only heater (ISC) abuse tests, and (d) only nail penetration tests.

However, some low-power high-energy-density cells also displayed high kJ/Ah but it is notable that these cells are expected to contain some Si in their anodes, such as the LG MJ1 cells [29]. Other important intrinsic properties to consider are the chemistry and the safety features of the cells, as these directly affect the progression of thermal runaway. The Saft-D-Cell-VES16 cells were the largest cells tested by volume and are thought to have more excess electrolyte for long-life applications than other cells tested. As discussed in previous work covering the Saft D-Cells [30], this may change the severity of thermal runaway by having more latent heat lost to evaporating the electrolyte, which was previously investigated by Ostanek et al. [16], and may account for the lower heat output per Ah of the Saft cells (~18 kJ/Ah).

For each of the FTRC tests, the ejected mass was also collected. A correlation appears when the capacity-normalized heat output (kJ/Ah) is plotted against the percent of the cells original mass ejected during thermal runaway, as shown in Fig. 3a. In general, cells that ejected more mass displayed higher total heat output (kJ/Ah). When the data were separated into the 3 distinct abuse types (heater non-ISC, heater ISC, and nail penetration) as shown in Fig. 3b–d, the correlation between ejected mass and heat output appeared to be most strong for the heater non-ISC tests in Fig. 3b, i.e., the tests involving off-the shelf commercial cells that are heated until thermal runaway occurred. While some cells group closely together for ejected mass and total heat, like the Sanyo 18650-A at the bottom left of Fig. 3b, other cells display a wide range of mass ejected and corresponding range of total heat emitted. For example, the "LG 18650 test cell (BV 220)" displayed 19 kJ/Ah heat output for 50 % mass ejection and 27 kJ/Ah for 85 % mass ejection, with many cells in between completing an approximately linear relationship between mass ejected and total heat output. The cause of this correlation will be explored in more detail later in this manuscript.

Some of the heater-ISC tests displayed a similar positive correlation between mass ejected and heat output, such as the "LG test cell (NBV 250)" shown in Fig. 3c whereas others such as the "Saft D-Cell VES16" and the "MOLICEL Test Cell (DW-Silver)" did not display enough of a distribution of mass ejection to determine any correlation.

The nail penetration cells in Fig. 3d displayed a distinctly different behavior than the heating tests. The nail tests displayed considerably lower variation in mass ejected and heat output, albeit for the small variation that they did display, a positive correlation between mass ejected and heat output was still observed. The low variation in mass ejected and heat output was shown in previous work [31] to be caused by the nail interfering with the thermal runaway process. Based on cells

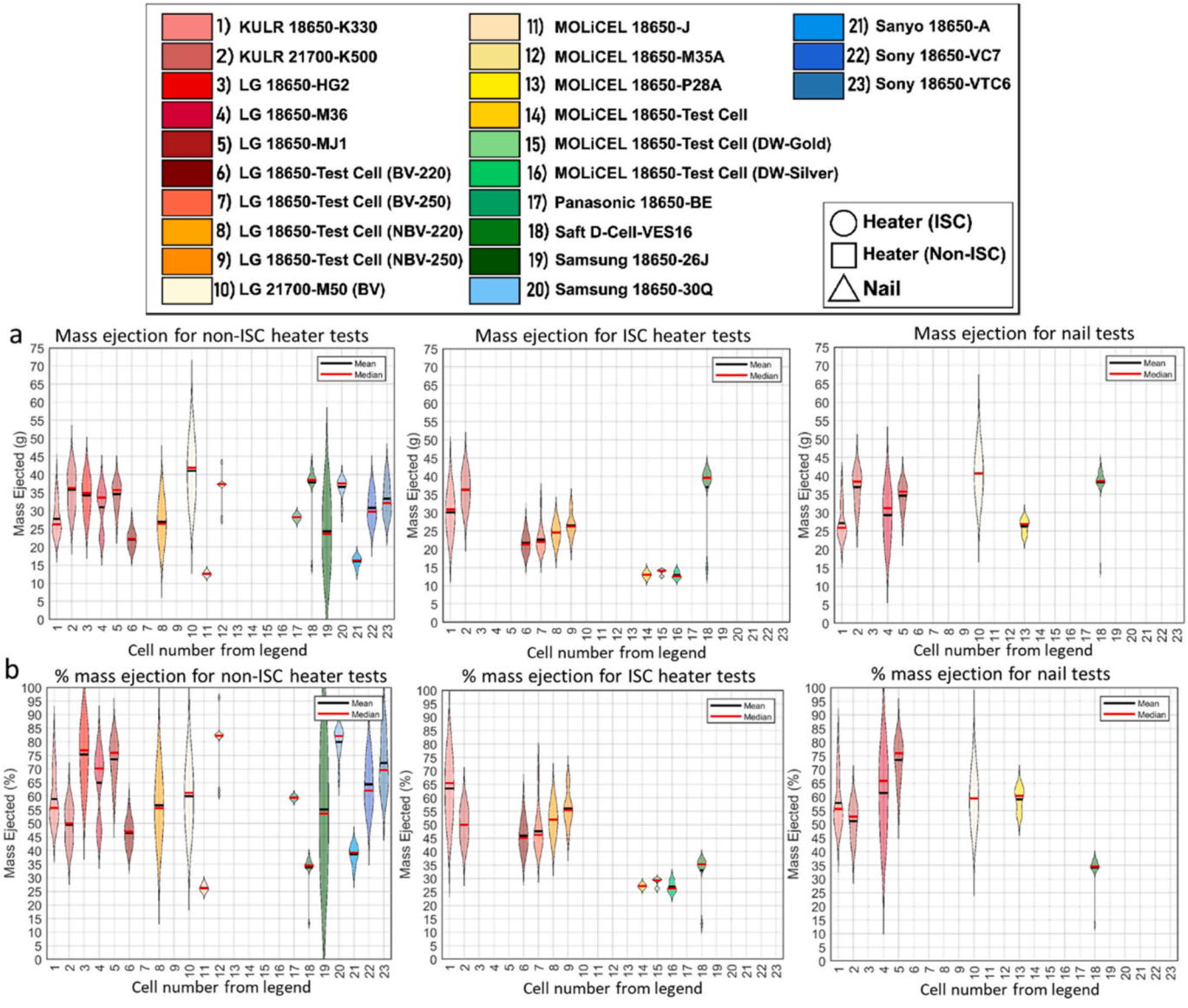

Fig. 4. (a) Absolute mass ejection in grams for the various cell types, and (b) the corresponding percent of the original mass of the cell that was ejected.

tested by the authors [31], the nail pins the electrode assembly inside the cell preventing it from shifting, clogging the vent, and causing a catastrophic rupture of the cell. The nail initiates thermal runaway across most layers of electrodes that it radially punctures, rather than thermal runaway spreading radially due to heat dissipation which was observed to be a slower process [31]. When the electrode assembly fluidizes during thermal runaway, the nail then continues to act as a baffle by disrupting the flow of ejecting fluidized material. Finally, the nail helped dissipate heat to outside the cell via conduction and also provided an additional hole for pressure relief. Another interesting trend observed in previous work [30] using the same data from the BFD showed that nail penetration tests showed increasingly more heat output for increasing diameter of cell due to the nail's influence on spreading thermal runaway across radial layers of electrode becoming increasingly influential on the rate of thermal runaway propagation for cells with more internal layers and larger diameters.

3.3. Correlation between heat output and mass ejection

The correlation of mass ejected and total heat output will be explored in greater detail in this section. Fig. 4a shows the distribution of mass ejected in absolute terms of grams, which includes only recovered mass and not the gaseous mass that escaped. Fig. 4b shows the equivalent data in percentage of the original mass of each cell. Most cells ejected around 25–40 g of material. As seen in Fig. 4b, this equated to between 50 and 85 % of each cell's mass being ejected. Some cells had a narrow distribution of mass ejected such as the Saft VES16 and all of the MOLICELs. Other cells had a very large distribution of mass ejected, such as the Samsung 26J and some of the LG cells. In additional to influencing the total heat output, a large mass ejection presents increased risk for other components outside the cell to become damaged and exacerbate the catastrophic failure.

To investigate the relationship between mass ejected and heat output, the mass and heat values for positive ejected material, cell body, and negative ejected material were separated and analyzed individually in Fig. 5 where the distinct heat measurements were plotted against their corresponding quantities of mass. There was a strong linear trend in all 3 scenarios of positive ejected mass, cell body mass (i.e., mass remaining in casing), and negative ejected mass. The positive ejected mass had a lot more data points and higher values than the negative ejected mass, which was due to most cells having a vent on the positive end of the cylindrical cell only. Cells that ejected mass via the negative end either had a bottom vent (planned negative ejection) or incurred a breach on the cell casing during thermal runaway (unplanned negative ejection).

It is notable that the slope of the line for ejected mass is considerably higher than the non-ejected mass or cell body. The slope here corresponds to the kJ of heat output per gram of material (kJ/g). The slopes for the positive and negative ejected masses were 2.41 and 2.82 kJ/g, whereas the slope for the cell body mass was 0.21 kJ/g. This indicates that ejected mass contributes more than 10 × the heat output per gram of material than the mass contained within the cell body, which explains the positive correlation between mass ejected and total heat output during thermal runaway observed in Fig. 3. A likely reason behind ejected mass contributing more heat during thermal runaway in the FTRC is due to the mass being ejected into a more oxygen rich environment than inside the cell. Assuming the mass is sufficiently hot, the excess atmospheric oxygen may facilitate thermal runaway reactions to run further to completion. However, the amount of excess oxygen is expected to be less inside the enclosed volume of the FTRC than if the mass was ejected into an open volume, such as into a large room. Mass contained within the cell body is likely to be more starved of oxygen and even though some of the cathode materials provide their own oxygen as part of their stoichiometry, it may not be enough for reactions to run to completion.

3.4. Linking thermal behavior to internal dynamics using high-speed radiography

For each type of cell in the BFD, a distribution of mass ejected and heat output was observed. Some cell models displayed a wider distribution than others, which raises the question of why cell behavior varies? Many of the tests in the BFD are accompanied by YouTube-hyperlinked high-speed radiography videos (2000–3000 fps) of the thermal runaway event during the FTRC test. These radiography videos provide a window into how thermal runaway initiated and propagated throughout the cell, and the timing of material fluidization and/or

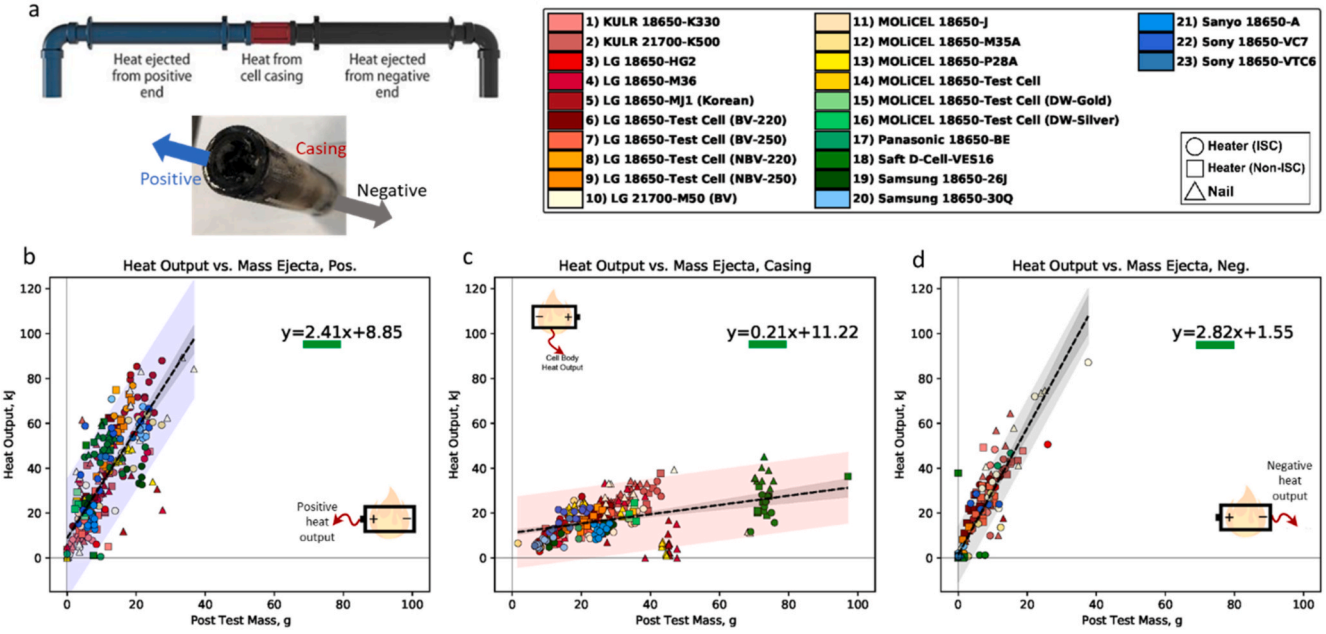

Fig. 5. (a) Illustration of FTRC as a visual guide for data. (b) Fractional heat output as a function of mass for positive ejected material, (c) material that remained within the cell casing, and (d) negative ejected material. A straight line is fit to each dataset and the corresponding linear equation is provided showing the differences in slope, i.e. the kJ/g of material.

ejection. This presents a unique opportunity to create a link between internal dynamics during thermal runaway and external measurements that are typically used to evaluate risks such as heat and mass ejection.

The Samsung 18650-26J model showed a high distribution of mass ejected and heat generated. What is particularly striking is the mass ejection data from this cell model as shown in Fig. 6a, which showed two distinct groupings of cells that ejected around 30–40 % of their mass (labelled as “Low mass ejection”) and cells that ejected 70–80 % of their mass (labelled as "High mass ejection”). On exploring the radiography videos of the thermal runaway and ejection process within the cell, a cause of this split became apparent. As a case study, we focus on tests “DLS 19 Dec Run006” and “DLS 19 Dec Run001”, as highlighted in Fig. 6a. Snapshots from the radiography videos for these tests are provided in Fig. 6b, and the full videos can be found in the BFD with their respective test-names shown above hyperlinked to YouTube. These cells are demonstrable of an interplay between time, thermal runaway progress, and mass ejection influencing the total heat and mass ejection of the cell. The “Low mass ejection” cell displayed a relatively long thermal runaway propagation within the cell over 1.5 s, while the “High mass ejection” cell ejected its electrode assembly within ~0.1 s after thermal runaway was observed to initiate. The “Low” cell retained most of its mass within the casing and thermal runaway propagated throughout the cell, the active materials fluidized, and a controlled release of pressure of fluids during the thermal runaway event occurred. The "High” cell experienced a violent rupture within 0.1 s of thermal runaway initiating, ejecting the entire electrode assembly all at once. This type of rupture was shown in previous work [9] to be caused by the vent of the cell becoming clogged and the cell releasing it’s header components and facilitating a total ejection of the electrode assembly before thermal runaway could propagate through the active material inside the cell casing. These and other radiography videos point to two factors that considerably influence the total heat generated; how much mass is ejected and when the mass is ejected during the thermal runaway process For example, if the mass ejects early during thermal runaway before the cell gets hot, then it may lead to a high mass ejection with low total heat output due to the temperature of the electrode assembly outside the cell not being high enough to bring reactions to completion. Conversely, if the cell ejects high mass later during the thermal runaway process when the cell contents are very hot, then reactions may continue for an extended period of time in the oxygen rich environment outside the cell. This highlights the interplay of time, thermal runaway progress, and mass ejection influencing the risks posed by the cell when it fails.

4. Conclusion

The BFD provides a valuable resource for assessing and understanding the variation in cell behaviors during thermal runaway. Comprising of over 300 tests of Li-ion cells conducted in a FTRC, many of which have accompanying high-speed synchrotron radiography, the BFD sheds light on the mass and heat ejection behavior of commercial cells under thermal and nail penetration abuse. Heat output increased with cell capacity, and heat output for each distinct cell model increased with increased mass ejected from the cell during thermal runaway. In general, higher power cells and cells with Si in their anode generated more heat per Ah than other cells.

For the cell designs evaluated here, it was also found that ejected mass emitted more heat per gram than non-ejected mass that remained in the cell casing, which is thought to be due to the ejected mass being exposed to a more oxygen rich environment that facilitated greater reaction completion. Non-ejected mass emitted around 0.21 kJ/g whereas ejected mass emitted around 2.6 kJ/g, i.e., >10 × more heat per gram was emitted by ejected mass. Each cell type also displayed a distinct magnitude of variation of behaviors, with some cells showing high consistency in mass ejected and heat generated, and other cells showing a high degree of variability. This emphasized the importance of evaluating the safety of cells using data from a high number of tests and raised the question of what causes such variability? Using high-speed radiography videos, it was seen that an interplay of time, thermal runaway progress, and mass ejection influenced the total heat output i.e., the dynamics of mass ejection during the thermal runaway process played a role in total heat output and the distribution of heat output. Some cells were shown to clog and eject their entire contents within 0.1 s after thermal runaway initiated, whereas other cells allowed thermal runaway to run to completion within the cell casing while continuously

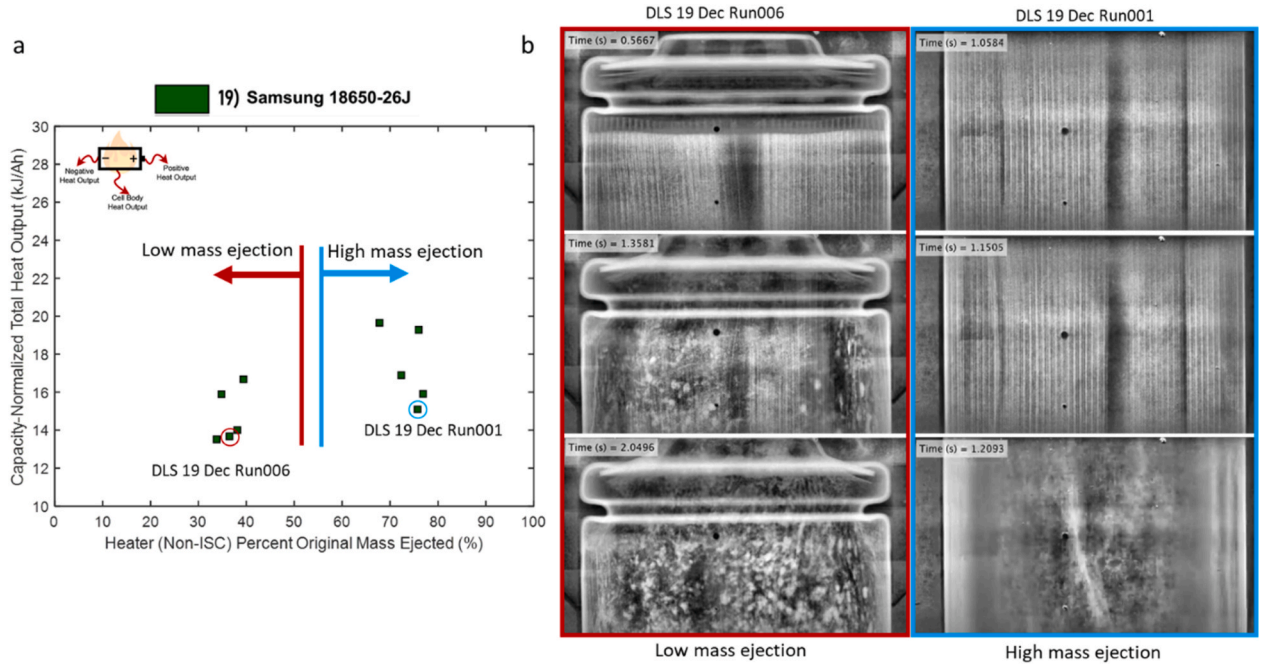

Fig. 6. (a) Isolated capacity-normalized heat output data for the Samsung 18650-26J showing a high variation in heat output and mass ejected. Two tests are labelled for a case study. (b) Corresponding radiography videos for the two labelled tests from the BFD showing differences in behavior of mass ejection, with one cell showing slow (over 1.5 s), gradual, and low mass ejection, and the other cell showing immediate (within 0.1 s) ejection of the entire electrode assembly.

ejecting fluidized material.

For engineers seeking to design safe battery systems, this work shows that it is important to understand the variation in thermal and mass ejection behaviors of cells. Of particular importance is understanding the outliers, where high heat generation or mass ejection are observed along with failures of the cell enclosure (side-wall breaching). The BFD contains enough information for numerous other analyses on the various cell types contained within than is presented here. The BFD will continue to be expanded by our team as we conduct further FTRC tests on new cell designs and is expected to be update in the near future with hundreds more additions. Engineers and researchers are encouraged to use this resource to help guide their cell selection decisions, to act as a benchmarking resource for their own internal evaluations, or to conduct further deep-dive analyses on correlations between internal cell behaviors during thermal runaway (via high-speed radiography) and the risks posed externally through heat and mass ejection.

Declaration of competing interest

The authors declare that they have no known competing financial interests or personal relationships that could have appeared to influence the work reported in this paper.

Data availability

Data is provided in open-access database on NREL's website

Acknowledgements

This work was authored by Alliance for Sustainable Energy, LLC, the manager and operator of the National Renewable Energy Laboratory for the U.S. Department of Energy (DOE) under Contract No. DE-AC36-08GO28308. The views expressed in the article do not necessarily represent the views of the DOE or the U.S. Government. The U.S. Government and the publisher, by accepting the article for publication, acknowledges that the U.S. Government retains a nonexclusive, paid-up, irrevocable, worldwide license to publish or reproduce the published form of this work, or allow others to do so, for U.S. Government purposes. These experiments were performed between beamlines ID19 at the ESRF (Grenoble, France) and I12 at Diamond Light Source (Harwell, UK). This work was carried out with the support of Diamond Light Source, instrument I12 (proposals MG24112, EE20903, EE17641). We are grateful to the ESRF and Diamond Light Source for allowing us to use their facilities. This work was also supported in part by the Faraday Institution (EP/S003053/1, Grant FIRG 058, FIRG 060 and FIRG 061) and the National Measurement System of the UK Department of Business, Energy and Industrial Strategy. PRS was supported by the Department of Science, Innovation and Technology (DSIT) and the Royal Academy of Engineering under the Chair in Emerging Technologies programme (CiET1718/59).

References

[1] B. Nykvist, M. Nilsson, Rapidly falling costs of battery packs for electric vehicles, Nature Clim. Change 5 (4) (2015) 329–332.
[2] NTSB *aircraft incident report, auxiliary power unit battery fire, Japan airlines boeing 787-8, JA829J*; PB2014-108867, January 7, 2014, National Transport Safety Board (2014).
[3] M. Gikas, J. Beilinson, Samsung investigation reveals new details about Note7 battery failures 2017. http://www.consumerreports.org/smartphones/samsung-investigation-new-details-note7-battery-failures/.
[4] J. Lamb, C.J. Orendorff, L.A.M. Steele, S.W. Spangler, Failure propagation in multi-cell lithium ion batteries, J. Power Sources 283 (2015) 517–523.
[5] A. Börger, J. Mertens, H. Wenzl, Thermal runaway and thermal runaway propagation in batteries: what do we talk about? J. Energy Storage 24 (2019) 100649.
[6] J. Deng, C. Bae, J. Marcicki, A. Masias, T. Miller, Safety modelling and testing of lithium-ion batteries in electrified vehicles, Nat. Energy 3 (4) (2018) 261–266.
[7] D.P. Finegan, E. Darcy, M. Keyser, B. Tjaden, T.M.M. Heenan, R. Jervis, J.J. Bailey, R. Malik, N.T. Vo, O.V. Magdysyuk, R. Atwood, M. Drakopoulos, M. DiMichiel, A. Rack, G. Hinds, D.J.L. Brett, P.R. Shearing, Characterising thermal runaway within lithium-ion cells by inducing and monitoring internal short circuits, Energy Environ. Sci. 10 (6) (2017) 1377–1388.
[8] D.P. Finegan, In-operando high-speed tomography of lithium-ion batteries during thermal runaway, Nat. Commun. 6 (2015).
[9] D.P. Finegan, E. Darcy, M. Keyser, B. Tjaden, T.M.M. Heenan, R. Jervis, J.J. Bailey, N.T. Vo, O.V. Magdysyuk, M. Drakopoulos, M.D. Michiel, A. Rack, G. Hinds, D.J. L. Brett, P.R. Shearing, Identifying the cause of rupture of Li-ion batteries during thermal runaway, Adv. Sci. 3 (2017) 1700369.
[10] A.W. Golubkov, D. Fuchs, J. Wagner, H. Wiltsche, C. Stangl, G. Fauler, G. Voitic, A. Thaler, V. Hacker, Thermal-runaway experiments on consumer Li-ion batteries with metal-oxide and olivin-type cathodes, RSC Adv. 4 (7) (2014) 3633–3642.
[11] W.Q. Walker, J.J. Darst, D.P. Finegan, G.A. Bayles, K.L. Johnson, E.C. Darcy, S. L. Rickman, Decoupling of heat generated from ejected and non-ejected contents of 18650-format lithium-ion cells using statistical methods, J. Power Sources 415 (2019) 207–218.
[12] D.P. Finegan, J. Darst, W. Walker, Q. Li, C. Yang, R. Jervis, T.M.M. Heenan, J. Hack, J.C. Thomas, A. Rack, D.J.L. Brett, P.R. Shearing, M. Keyser, E. Darcy, Modelling and experiments to identify high-risk failure scenarios for testing the safety of lithium-ion cells, J. Power Sources 417 (2019) 29–41.
[13] S.J. Drake, M. Martin, D.A. Wetz, J.K. Ostanek, S.P. Miller, J.M. Heinzel, A. Jain, Heat generation rate measurement in a Li-ion cell at large C-rates through temperature and heat flux measurements, J. Power Sources 285 (2015) 266–273.
[14] K. Shah, S.J. Drake, D.A. Wetz, J.K. Ostanek, S.P. Miller, J.M. Heinzel, A. Jain, Modeling of steady-state convective cooling of cylindrical Li-ion cells, J. Power Sources 258 (2014) 374–381.
[15] B. Coleman, J. Ostanek, J. Heinzel, Reducing cell-to-cell spacing for large-format lithium ion battery modules with aluminum or PCM heat sinks under failure conditions, Appl. Energy 180 (2016) 14–26.
[16] J.K. Ostanek, W. Li, P.P. Mukherjee, K.R. Crompton, C. Hacker, Simulating onset and evolution of thermal runaway in Li-ion cells using a coupled thermal and venting model, Appl. Energy 268 (2020) 114972.
[17] A. Kriston, A. Podias, I. Adanouj, A. Pfrang, Analysis of the effect of thermal runaway initiation conditions on the severity of thermal runaway—numerical simulation and machine learning study, J. Electrochem. Soc. 167 (9) (2020) 090555.
[18] W. Li, J. Zhu, Y. Xia, M.B. Gorji, T. Wierzbicki, Data-Driven safety envelope of lithium-ion batteries for electric vehicles, Joule 3 (11) (2019) 2703–2715.
[19] D.P. Finegan, J. Zhu, X. Feng, M. Keyser, M. Ulmefors, W. Li, M.Z. Bazant, S. J. Cooper, The application of data-driven methods and physics-based learning for improving battery safety, Joule 5 (2) (2020) 316–329.
[20] D.P. Finegan, S.J. Cooper, Battery safety: data-driven prediction of failure, Joule 3 (11) (2019) 2599–2601.
[21] K.A. Severson, P.M. Attia, N. Jin, N. Perkins, B. Jiang, Z. Yang, M.H. Chen, M. Aykol, P.K. Herring, D. Fraggedakis, M.Z. Bazant, S.J. Harris, W.C. Chueh, R. D. Braatz, Data-driven prediction of battery cycle life before capacity degradation, Nat. Energy 4 (5) (2019) 383–391.
[22] Y. Zhang, Q. Tang, Y. Zhang, J. Wang, U. Stimming, A.A. Lee, Identifying degradation patterns of lithium ion batteries from impedance spectroscopy using machine learning, Nat. Commun. 11 (1) (2020) 1706.
[23] P.M. Attia, A. Grover, N. Jin, K.A. Severson, T.M. Markov, Y.-H. Liao, M.H. Chen, B. Cheong, N. Perkins, Z. Yang, P.K. Herring, M. Aykol, S.J. Harris, R.D. Braatz, S. Ermon, W.C. Chueh, Closed-loop optimization of fast-charging protocols for batteries with machine learning, Nature 578 (7795) (2020) 397–402.
[24] B. Saha, K. Goebel, Battery Data Set. NASA Ames Research Center, NASA Ames program data repository, Moffett Field CA, 2007.
[25] J.E. Harlow, X. Ma, J. Li, E. Logan, Y. Liu, N. Zhang, L. Ma, S.L. Glazier, M.M. E. Cormier, M. Genovese, S. Buteau, A. Cameron, J.E. Stark, J.R. Dahn, A wide range of testing results on an excellent lithium-ion cell chemistry to be used as benchmarks for new battery technologies, J. Electrochem. Soc. 166 (13) (2019) A3031–A3044.
[26] Battery Failure Databank, National Renewable Energy Laboratory, 2021. https://www.nrel.gov/transportation/battery-failure.html.
[27] X. Feng, S. Zheng, D. Ren, X. He, L. Wang, H. Cui, X. Liu, C. Jin, F. Zhang, C. Xu, H. Hsu, S. Gao, T. Chen, Y. Li, T. Wang, H. Wang, M. Li, M. Ouyang, Investigating the thermal runaway mechanisms of lithium-ion batteries based on thermal analysis database, Appl. Energy 246 (2019) 53–64.
[28] M. Keyser, E. Darcy, D. Long, A. Pesaran, Passive safety device and internal short tested method for energy storage cells and systems, Sep 22, 2015, U.S. patent 9142829B2 (2015).
[29] X. Li, A.M. Colclasure, D.P. Finegan, D. Ren, Y. Shi, X. Feng, L. Cao, Y. Yang, K. Smith, Degradation mechanisms of high capacity 18650 cells containing Si-graphite anode and nickel-rich NMC cathode, Electrochim. Acta 297 (2019) 1109–1120.
[30] M. Sharp, J.J. Darst, P. Hughes, J. Billman, M. Pham, D. Petrushenko, T.M. M. Heenan, R. Jervis, R. Owen, D. Patel, D. Wenjia, H. Michael, A. Rack, O. V. Magdysyuk, T. Connolley, D.J.L. Brett, G. Hinds, M. Keyser, E. Darcy, P. R. Shearing, W. Walker, D.P. Finegan, Thermal runaway of Li-ion cells: how internal dynamics, mass ejection, and heat vary with cell geometry and abuse type, J. Electrochem. Soc. 169 (2) (2022) 020526.
[31] D.P. Finegan, B. Tjaden, M.M. Heenan, T. Jervis, R, M.D. Michiel, A. Rack, G. Hinds, D.J.L. Brett, P.R. Shearing, Tracking internal temperature and structural dynamics during nail penetration of lithium-ion cells, J. Electrochem. Soc. 164 (13) (2017) A3285–A3291.